20th International Sacramento Peak Summer Workshop
Advanced Solar Polarimetry - Theory, Observation, and Instrumentation
ASP Conference Series, Vol. 236, 2001
M. Sigwarth, ed.

A Synthesis Code for Forbidden Coronal Lines

P. G. Judge, R. Casini

High Altitude Observatory, National Center for Atmospheric Research,[1]
P.O. Box 3000, Boulder CO 80307-3000, USA

Abstract. We describe a `Fortran-77` program for the synthesis of Stokes profiles of forbidden lines such as [Fe XIII] 1074.7nm, formed in magnetic dipole transitions under coronal conditions. The lines are assumed to be optically thin, excited by (anisotropic) photospheric radiation and thermal particle collisions. The inclusion of particle collisions extends the work of Casini & Judge (1999), which built upon the work of Charvin, Sahal-Bréchot, and House in the 1960's and 1970's. This new work is spurred on by the need to measure properties of coronal magnetic fields, ultimately to address fundamental questions concerning the storage and release of magnetic free energy in the corona. Compared with radio and Hanle-effect techniques, measurements of the complete Stokes vector of forbidden lines offer the possibility of constraining components of the magnetic field direction as well as magnitude and sign of the longitudinal field strength, but the polarization magnitudes are small. The computer program has been developed as a tool for assessing the potential for making such measurements, in particular to help to determine the best strategies for the development of new instruments following the recent detection of the longitudinal Zeeman effect in the [Fe XIII] 1074.7 nm line by Lin, Penn and Tomczyk (2000).

1. Introduction

The advent of the Space Age has brought major advances in our knowledge of the Sun. The widely accepted idea of magnetically controlled loop structures as fundamental building blocks of the corona was established soon after SKYLAB revealed images of the X-ray corona; ground and space-borne coronagraphs have accumulated large statistical databases of properties of coronal mass ejections; Hα and EUV imagers have revealed tantalizing pictures of the role of magnetically sheared structures in energizing the corona. Yet coronal physics remains, as it has been for many decades, hampered by lack of quantitative knowledge of the magnetic field permeating the corona.

Synoptic measurements of the coronal magnetic field have the potential to reveal the basic response of the corona to the (sub)-photospheric driving

[1]The National Center for Atmospheric Research is sponsored by the National Science Foundation

motions and emergence of new magnetic flux. In the 1970s, coronagraphic measurements of linear polarization of forbidden coronal lines, particularly from Pic du Midi (Arnaud 1982) and Sacramento Peak (Querfeld & Smartt 1984, Arnaud & Newkirk Jr. 1987), were made, revealing directions of the coronal magnetic field projected onto the plane of the sky ("POS"). The magnitude of linear polarization was less by a factor of three than homogeneous models predicted, and the direction was found to be predominantly radial. By today's standards, these measurements are quite crude, limited by small instrumental apertures ($\leq$ 40cm diameter), large pixels ($\approx$ 1 arcmin^2 projected areas), and small detector arrays. Nevertheless, these measurements represent the most complete database available for studies of the coronal magnetic field.

We can currently only imagine that answers will be forthcoming to several important questions. Why did the early measurements yield low polarization magnitudes and mostly radial directions? How good are extant extrapolations of magnetic fields from photosphere to corona? What magnetic configurations lead to CME launch/flares? How does the coronal field respond to/affect the 11 year polarity change? What is the real relationship between the observed "plasma loops" and the magnetic fields (e.g., Fort & Martres 1974)?

We expect that our imagination will soon be curtailed by real observational constraints. Indeed, considerable progress has been made using disk and limb observations of sunspots—regions of very strong magnetic fields—using the gyro-resonance technique (predicted by Ginzburg & Zheleznyakov 1961, and later observed by, e.g., Kundu et al. 1980). However, outside of these regions, we have only just begun to explore the possibilities. Radio observations under conditions formed outside of the gyro-resonant regime are possible in weaker fields associated with plages, quiet Sun, and even coronal holes (e.g., Shibasaki, this proceedings), both on and off the disk, and should be vigorously pursued. Disk (and even some limb) radio observations suffer from ambiguities arising from the unknown optical depth of the emitting plasma. However, these measurements can (even in principle) only yield line-of-sight field strengths. Infrared observations, restricted to measurements above the limb because of the brightness of the solar disk, nevertheless hold the potentially greater possibility of constraining not only this quantity—as demonstrated recently by the detection of the Zeeman effect in the [Fe XIII] 1074.7 nm line (Lin et al. 2000)—but also the direction of the field in the POS through the (much easier) linear polarization measurements (e.g., Arnaud 1982). The direction of the field provides one with a much greater chance of constraining the magnetic free energy, by setting constraints on the current density $\vec{j} = \vec{\nabla} \times \vec{B}$.

Still more techniques can be used: Hanle effect in prominences (limb or disk capabilities exist); Hanle effect in special UV lines (limb only, Raouafi, this proceedings); Faraday rotation of cosmic/spacecraft radio sources (limb only). These avenues should be pursued. This paper focuses on the use of forbidden coronal lines.

2. The computer program

2.1. Underlying physics

A partial discussion of the formation of coronal M1[1] lines is given by Casini & Judge (1999, and erratum in Casini & Judge 2000). In that paper, the non-relativistic quantum theory of line formation of Landi Degl'Innocenti (1983, 1984) was adopted, and the formalism of the irreducible spherical components of the atomic density matrix was used to illuminate the essential physics by bringing out the basic symmetries in the simplest way (Sahal-Bréchot 1977; Landi Degl'Innocenti 1984; Trujillo-Bueno, this proceedings). This approach is formally equivalent to the more familiar one, based on the representation of the atomic density matrix in terms of eigenfunctions of the atomic Hamiltonian, that was used by House (1977). The `Fortran-77` program described here is based on the Casini & Judge formalism. The code incorporates some appropriate physical regimes in the corona, by making several simplifying assumptions which have been laid out clearly, e.g., by Sahal-Bréchot (1974a, 1974b, 1977). The most important are: (1) The corona is optically thin to all radiation and is irradiated by spectrally featureless, unpolarized radiation from the underlying atmosphere. (2) The atomic states involved in the forbidden line transitions have natural widths much less than Zeeman splittings. The ionic density matrix in the atomic eigenfunction representation (the "standard basis"), $\rho(M, M')$, is therefore diagonal in (M, M'), if we take the direction of the magnetic field as the quantization axis. In the irreducible spherical tensor representation, this means that only the coefficients of the density matrix ρ^K_Q with $Q = 0$ are non-zero. (3) All other states (including more highly excited levels which may have natural widths $\approx$ Zeeman splittings) are populated "naturally" (equal magnetic substate populations) since they always lie high enough in energy to be populated primarily by isotropic particle impact and ionic recombination. Therefore, coherences (ρ^K_Q, $Q \neq 0$) are negligible and need not be calculated. (4) Zeeman splittings are much less than Doppler widths which in turn are much less than the fine structure splitting. Emission coefficients need therefore be retained only to first order in the ratio of Zeeman splitting to Doppler width. (5) Colliding particles have Maxwellian (hence isotropic) distribution functions.
In terms of the density matrix, we can define atomic *population, orientation,* and *alignment* of a level specified by quantum numbers (αJ) respectively by:

$$\rho^0_0(\alpha J) = \sum_M \rho_{\alpha J}(M, M) , \quad (1)$$

$$\rho^1_0(\alpha J) = \frac{\sqrt{3}}{\sqrt{\Pi_J}} \sum_M M\, \rho_{\alpha J}(M, M) , \quad (2)$$

$$\rho^2_0(\alpha J) = \frac{\sqrt{5}}{\sqrt{\Pi_J (2J-1)(2J+3)}} \sum_M [3M^2 - J(J+1)]\, \rho_{\alpha J}(M, M) , \quad (3)$$

[1] M1 means magnetic dipole, E1 electric dipole, E2 electric quadrupole, etc..

where $\Pi_J = J(J+1)(2J+1)$. These equations give the density matrix coefficients expressed in the irreducible spherical tensor formalism as functions of the (diagonal) density matrix coefficients in the standard basis. The incident radiation, being directed but unpolarized, can generate only *population* and *alignment*, and hence only Stokes I, Q, U. The Zeeman effect generates predominantly Stokes V (linear polarization in the lines is dominated by resonance scattering), but the presence of a non-zero atomic alignment leads to a systematic modification of the well-known magnetograph formula (Casini & Judge 1999).

These conditions lead to the following qualitative picture for the interpretation of forbidden coronal lines. *Linear polarization* measurements rotated to a frame where $Q \neq 0$ and $U = 0$ yield the (projected) direction of the magnetic field in the POS with, in principle, an ambiguity of 90°. This ambiguity arises because the magnitude of the linear polarization is proportional to the "alignment factor" $\sigma_0^2(\alpha J) = \rho_0^2(\alpha J)/\rho_0^0(\alpha J)$, which in turn is (approximately) proportional to the "anisotropy factor" of the radiation field, J_0^2/J_0^0, evaluated in the frame of reference of the magnetic field. J_0^2 changes sign as the inclination angle of the magnetic field with the solar vertical, ϑ_B, passes through the Van Vleck angle ($\approx 54°.7$; e.g., House 1977). Thus, because the sign of $\sigma_0^2(\alpha J)$ is in principle not known, an additional ambiguity arises besides the well-known 180°-ambiguity of all polarization measurements. *Circular polarization* depends on $[1 + a\,\sigma_0^2(\alpha J)]/[1 + b\,\sigma_0^2(\alpha J)]$ times the magnetograph formula, where a depends on atomic parameters and b depends also on ϑ_B [Casini & Judge 1999, eq. (41)]. Thus, Stokes Q and U have contributions from atomic alignment and yield constraints on the direction of $\vec{B}$ in the POS; Stokes V is modified by the presence of atomic alignment but the magnetograph formula can yield constraints on the magnitude and direction of the magnetic field along the line-of-sight (LOS).

2.2. Treatment of collisional processes

The physics underlying the code is complete except for the lack of knowledge of some collisional coefficients. In general, collisions must be described in terms of coefficients (for example the inelastic[2] collision coefficient C_I) such that, in the standard basis,

$$\frac{\mathrm{d}}{\mathrm{d}t}\,\rho_{\alpha J}(M, M') = \sum_{\alpha_\ell J_\ell M_\ell, M'_\ell} C_I(\alpha J M M', \alpha_\ell J_\ell M_\ell M'_\ell)\;\rho_{\alpha_\ell J_\ell}(M_\ell, M'_\ell) \qquad (4)$$

represents the rate of change of the density matrix element $\rho_{\alpha J}(M, M')$ arising from collisional processes that induce transitions from the density matrix element $\rho_{\alpha_\ell J_\ell}(M_\ell, M'_\ell)$. Quantum numbers $(\alpha_\ell J_\ell)$ denote any atomic level having energy lower than level (αJ). Because coherences (off diagonal elements with $M \neq M'$) can be neglected in our problem, eq. (4) becomes

$$\frac{\mathrm{d}}{\mathrm{d}t}\,\rho_{\alpha J}(M, M) = \sum_{\alpha_\ell J_\ell M_\ell} C_I(\alpha J M, \alpha_\ell J_\ell M_\ell)\;\rho_{\alpha_\ell J_\ell}(M_\ell, M_\ell)\;, \qquad (5)$$

[2]By inelastic, superelastic, and elastic processes, we refer to the cases where the final state of the ion is in a higher, lower, and same level, respectively, as the initial state (αJ).

which contains the more familiar coefficient $C_I(\alpha JM, \alpha_\ell J_\ell M_\ell)$ describing the rate at which the sub-level population is transferred from sub-level $(\alpha_\ell J_\ell M_\ell)$ to a higher sub-level (αJM). These coefficients can easily be transformed into the form needed for the irreducible spherical tensor formalism (Landi Degl'Innocenti & Landolfi 2001), yielding an equation of the form

$$\begin{aligned}\frac{\mathrm{d}}{\mathrm{d}t}\rho^K_0(\alpha J) &= \sum_{\alpha_\ell J_\ell}\sqrt{\frac{2J_\ell+1}{2J+1}}\,C_I^{(K)}(\alpha J,\alpha_\ell J_\ell)\;\rho^K_0(\alpha_\ell J_\ell)\\ &+ \sum_{\alpha_u J_u}\sqrt{\frac{2J_u+1}{2J+1}}\,C_S^{(K)}(\alpha J,\alpha_u J_u)\;\rho^K_0(\alpha_u J_u) \qquad (6)\\ &- \left[\sum_{\alpha_u J_u} C_I^{(0)}(\alpha_u J_u,\alpha J)+\sum_{\alpha_\ell J_\ell} C_S^{(0)}(\alpha_\ell J_\ell,\alpha J)+D^{(K)}(\alpha J)\right]\rho^K_0(\alpha J)\end{aligned}$$

that describes the total rate of change of $\rho^K_0(\alpha J)$ induced by inelastic (C_I), superelastic (C_S), and elastic (C_E) collisional processes. In order, the terms on the RHS of eq. (6) correspond to the terms $C^{(3)}$, $C^{(5)}$, $C^{(6)}$, $C^{(2)}$, and $C^{(0)}$ in eq. (20) of Casini & Judge (1999). $D^{(K)}(\alpha J) = C_E^{(0)}(\alpha J) - C_E^{(K)}(\alpha J)$ are called depolarizing rates due to elastic collisions. This equation shows that (isotropic) collisions couple density matrix elements of the same tensor order K.

Unfortunately, these coefficients [e.g., $C_I(\alpha JM, \alpha_\ell J_\ell M_\ell)$] are, apart from special cases (e.g., the treatment of proton collisions within the ground terms of Fe XIII and Fe XIV by Landman 1975), not known. Instead we have adopted the following approximate treatment, after Landi Degl'Innocenti & Landolfi (2001):

1. Initialize all collisional rates to zero.
2. Assume that electrons dominate the collision rates.
3. For inelastic and superelastic transitions satisfying E1 or E2 selection rules (e.g., in Fe XIII, the E1 transition $3s^2\ 3p^2\ {}^3P_1 \rightarrow 3s\ 3p^3\ {}^3D^o_1$ has a wavelength of 35.9nm), assume that the cross section is dominated by the lowest order multipole, $\tilde{K}$, in the expansion of the Coulomb potential, and adopt the appropriate rate coefficient, $C^{(0)}_{I,S}$, from the literature (e.g., the CHIANTI database of Dere et al. 1997). With this approximation, it can be shown (Landi Degl'Innocenti & Landolfi 2001), using symmetry arguments, that

$$C_I^{(K)}(\alpha J,\alpha_\ell J_\ell) \approx (-1)^K \frac{\begin{Bmatrix} J & J & K \\ J_\ell & J_\ell & \tilde{K}\end{Bmatrix}}{\begin{Bmatrix} J & J & 0 \\ J_\ell & J_\ell & \tilde{K}\end{Bmatrix}}\, C_I^{(0)}(\alpha J,\alpha_\ell J_\ell), \qquad (7)$$

and, analogously,

$$C_S^{(K)}(\alpha J,\alpha_u J_u) \approx (-1)^K \frac{\begin{Bmatrix} J & J & K \\ J_u & J_u & \tilde{K}\end{Bmatrix}}{\begin{Bmatrix} J & J & 0 \\ J_u & J_u & \tilde{K}\end{Bmatrix}}\, C_S^{(0)}(\alpha J,\alpha_u J_u). \qquad (8)$$

4. Equations (7) and (8) contain all the information needed to compute the inelastic and superelastic components of eqn. (6) in terms of the traditional fine structure rate coefficients $C^{(0)}_{I,S}$ and their leading multipole order $\tilde{K}$.

5. Elastic collisions should be treated but have been omitted thus far.

These approximations may not be as poor as a first inspection might suggest. For example, under "standard" conditions (lines formed close to ionization equilibrium conditions, with equal proton and electron temperatures) the effects of proton collisions are small. E1 transitions induced by electron impact to levels of opposite parity to the ground configuration occur at a much faster rate (e.g. Sahal-Bréchot 1974b). Such levels decay in a "cascade" to the ground levels. This process in fact dominates the net collision rates between levels of the ground term (Pecker & Thomas 1962). However, proton collision rates increase rapidly with increasing temperature. Neglect of elastic collision rates is a more serious omission, which will be addressed soon.

Uncertainties in collision rates influence the atomic population and alignment [eqs. (1) and (2)], which mainly influence just the *magnitude* of the linear polarization. The *direction* of the linear polarization is not affected, and the magnitude of circular polarization is influenced only in proportion to the ratio of the alignment to the population. Thus the POS direction and (probably) the LOS field strength should be quite insensitive to these uncertainties.

2.3. Code structure, performance

The code consists of two main parts. The first part is a subroutine `START` which reads atomic data, opens files, defines the 3D grid and defines a few simple options (which wavelengths to output to file, whether full line profiles are output, a limiting plasma density below which calculations are skipped, etc.). The second part is a repeated call to `M1SYNTH` for each LOS. In each cell along the LOS, `M1SYNTH` calls a routine `CORONA` which calls a user-defined routine to return the vector magnetic field, electron density and temperature, hydrogen density, vector velocity, microturbulent velocity all as a function of vector position relative to Sun center. Routines are then called to compute line profiles, collisional rate coefficients and radiation fields in each grid cell, and the statistical equilibrium (S.E.) equations are set up and solved. The emission coefficients are constructed in each cell along the LOS and integrated using the trapezoidal formula.

With the small ($\leq$ 8 level) atomic models used so far, most of the CPU time is spent building the S.E. equations. Substantial further optimization may be possible but has not been explored. It requires very little RAM (1.6 MByte is sufficient for an 8 level Fe XIII ion). On a 233 MHz Pentium MMX, running Linux with the `g77` compiler, a 3 level atom (9 substates) takes 0.006 sec per cell, or 1.6 hours for a $100 \times 100 \times 100$ grid. An 8 level atom (30 substates) requires 0.04 sec per cell, 11 hours for a $100 \times 100 \times 100$ grid. Substantial savings are made by skipping cells containing little plasma, for instance if the corona is basically void, dominated by loops. The code (radiative part) has been checked against analytical results for a 3 level atomic model.

Fig. 1 shows computed Stokes profiles for a dipolar field in which just three "flux tubes" have plasma within them. Reasonable physical parameters were

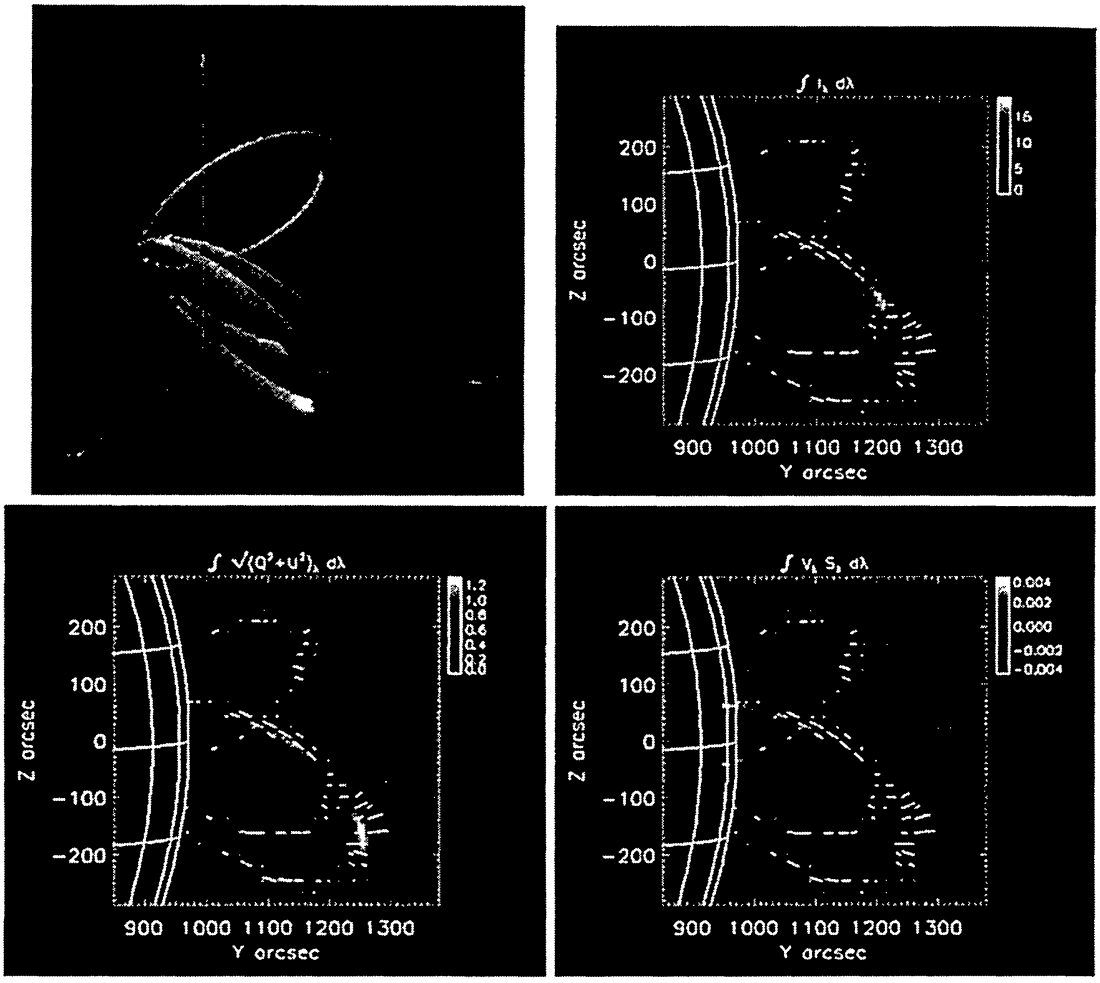

Figure 1. Computed polarization of the [Fe XIII] 1074.7 nm line (assuming zero flow velocity). Top left panel: distribution of plasma density (field lines are directed along the "tubes"); other panels: computed Stokes data (in erg cm^{-2} s^{-1} sr^{-1}). Lines show the direction of linear polarization.

used ($|B| \approx 2$ G at the loop tops, base electron density $\approx 10^8$ cm^{-3}, temperature $\approx$ 2 10^6K, 20 km s^{-1} microturbulence, no flows). The plotted quantities I, P, V are, respectively, wavelength-integrated intensity, linear polarization, and "signed" circular polarization, $V = \int V_\lambda S_\lambda \, \mathrm{d}\lambda$, with $S_\lambda = \mathrm{sgn}(\lambda - \lambda_0)$, where λ_0 is the line center. Note that $P \approx 0.1\, I$ and $|V| \approx 10^{-4}\, I$.

3. Conclusions and Future Work

Stokes profiles of M1 emission lines can be efficiently computed, including most of the essential physical processes accurate to first order in the expansion of the emission coefficients with frequency. The weakest part of the formalism arises from incomplete knowledge of collision rates, but these affect just the magnitude of the linear polarization and they enter only as a small correction to Stokes V

profiles. Thus, the derivable properties of the magnetic fields (direction in the POS, magnitude and direction along the LOS) can be determined reasonably well, in spite of this.

So far only simple, potential fields have been explored. In the short term we anticipate including a more complete treatment of collisions, making quantitative comparisons with earlier work (I, Q, U only), building realistic noise models for instrument development (e.g., the ATST project), and investigating a variety of spectral lines. We will study different potential field configurations, for example the prominence cavity/streamer models of Low (1986), and current-carrying field configurations. Lastly, we intend to examine the "data content problem" from the inverse vs. forward perspectives, including tomographic techniques.

In the long term, hopefully after suitable instrument development, we hope to confront measurements with simulations built, for example, on extrapolation of photospheric field measurements, and look for changes in magnetic fields before/after CME launch and/or flare eruption.

References

Arnaud, J. 1982, A&A 112, 350

Arnaud, J., Newkirk Jr., G. 1987, A&A 178, 263

Casini, R., Judge, P. G. 1999, ApJ 522, 524

Casini, R., Judge, P. G. 2000, ApJ 533, 574

Dere, K. P., Landi, E., Mason, H. E., Monsignori Fossi, B. C., Young, P. R. 1997, A&AS 125, 149

Fort, B., Martres, M. J. 1974, A&A 33, 249

Ginzburg, V., Zheleznyakov, V. V. 1961, Soviet Astr.-AJ 5, 1

House, L. L. 1977, ApJ 214, 632

Kundu, M. R., Schmahl ,E. J., Gerassimenko, M. 1980, A&A 82, 265

Landman, D. A. 1975, A&A 43, 285

Landi, Degl'Innocenti E. 1983, Sol. Phys. 85, 3

Landi, Degl'Innocenti E. 1984, Sol. Phys. 91, 1

Landi, Degl'Innocenti E., Landolfi, M. 2001, Polarization in Spectral Lines, in preparation

Lin, H., Penn, M. J., Tomczyk, S. 2000, ApJ 541, 83

Low, B. C. 1986, ApJ 310, 953

Pecker, J. C., Thomas, R. N. 1962, Ann. Astrophys. 25, 100

Querfeld, C. W., Smartt, R. N. 1984, Sol. Phys. 91, 299

Sahal-Bréchot, S. 1974a, A&A 32, 147

Sahal-Bréchot, S. 1974b, A&A 36, 355

Sahal-Bréchot, S. 1977, ApJ 213, 887